INVESTIGATION OF REVERSE TAPER TO OPTIMIZE THE DEGREE OF POLARIZATION FOR THE DELTA UNDULATOR AT THE LCLS*

J. MacArthur†, A. Marinelli, A. Lutmann, T. Maxwell, H.-D. Nuhn, D. Ratner, Z. Huang
SLAC, Menlo Park, CA 94025, USA

Abstract

A 3.2 m adjustable phase Delta undulator will soon be installed on the last girder of the LCLS undulator line. The Delta undulator will act as an afterburner terminating the 33 undulator line, providing arbitrary polarization control to users. Two important figures of merit for users will be the degree of polarization and the x-ray yield. In anticipation of this installation, machine development time at the LCLS was devoted to maximizing the final undulator x-ray contrast and yield with a standard canted pole planar undulator acting as a stand in for the Delta undulator. Following the recent suggestion [1] that a reverse taper in the main undulator line could suppress linearly polarized light generated before an afterburner while still producing the requisite microbunching, we report on a reverse taper study at the LCLS wherein a yield contrast of 15 was measured along the afterburner. We also present 1D simulations comparing the reverse taper technique to other schemes.

INTRODUCTION

Circularly polarized soft x-ray radiation is used to probe a variety of material properties, from the electronic structure of magnetic substances [2] to the chirality of biomolecules [3]. Off plane synchrotron radiation [4] and helical undulator radiation [5] have supplied circularly polarized x-rays to synchrotron users for several decades. High quality circularly polarized radiation from FEL facilities is limited to energies at or below the XUV [6], though thin magnetized films have been used to produce circularly polarized soft x-rays at the cost of several orders of magnitude in intensity [7].

A Delta undulator [8] is currently being constructed [9] at the LCLS to address this shortcoming. Unlike canted pole or adjustable gap devices, the Delta is an adjustable phase undulator [10] wherein the longitudinal position of four opposing magnetic arrays is varied to adjust the axial magnetic field strength and helicity. The result is full polarization control – linear, circular, and elliptically polarized light can be produced. The Delta undulator at LCLS will operate in the 300-2000 eV region, extending availability of circularly polarized FEL sources into the soft x-ray. This 3.2 m device will replace the final planar undulator in the 33 undulator-line at LCLS.

The Delta undulator is only 1.5-2 gain LCLS gain lengths long, not nearly long enough reach FEL saturation. Instead, the Delta will act as an afterburner, as seen in Fig. 1. In this configuration, the electron beam is microbunched in a long planar undulator before entering the Delta.

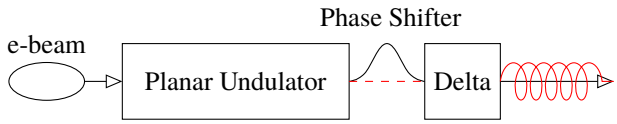

Figure 1: Schematic representation of the Delta undulator in the afterburner configuration. The beam is microbunched in the planar undulator, and a small amount of plane polarized radiation seeds the Delta after an optimum phase shift (red, dashed). The Delta produces circularly polarized x-rays (red, solid).

If the Delta undulator is configured with a helical field, the degree of circular polarization will be dictated by the ratio of the power produced in the Delta and the power produced in the planar undulator. To be more precise, the polarization of light is commonly characterized by the four Stokes parameters. In terms of the complex electric field, these parameters are [11]

$$
\begin{aligned}
s_0 &= \left\langle E_x E_x^* + E_y E_y^* \right\rangle = I_x + I_y \\
s_1 &= \left\langle E_x E_x^* - E_y E_y^* \right\rangle = I_x - I_y \\
s_2 &= \left\langle E_x E_y^* + E_y E_x^* \right\rangle = I_{45^\circ} - I_{-45^\circ} \\
s_3 &= i \left\langle E_x E_y^* - E_y E_x^* \right\rangle = I_{\mathrm{RCP}} - I_{\mathrm{LCP}},
\end{aligned}
$$

where $\langle\rangle$ indicates a time average over the pulse duration. The two figures of merit relevant to circularly polarized light from a helical undulator are the average power $P = \int s_0 \, dxdy$, and the degree of circular polarization, s_3/s_0.

Several schemes have been proposed to maximize the average power and $|s_3|/s_0$. A reverse taper can be applied to the planar undulator to suppress background radiation [1], the longer undulator and afterburner may be placed in a crossed-undulator configuration [12, 13], and the resonant frequency of the afterburner may be tuned to the second harmonic of the planar undulator [14]. In this paper we compare the reverse taper scheme to others in a 1D framework and report on an experimental investigation of the reverse taper scheme at LCLS.

1D COMPARISON

The resonant wavelength λ_r in an FEL is given as

$$
\lambda_r(z) = \frac{\lambda_u}{2\gamma^2}\left(1 + a_u^2(z)\right), \qquad (1)
$$

where λ_u is the undulator period and γ is the Lorentz factor. The rms undulator parameter $a_u = e\lambda_u B_{\mathrm{rms}}/2\pi mc$ is given

* Work supported by U.S. DOE Office of Basic Energy Sciences under Contract No. DE-AC02-76SF00515.
† jmacart@slac.stanford.edu

ISBN 978-3-95450-133-5

in terms of the on-axis rms magnetic field strength B_{rms}. Eq. 1 is valid for planar and helical undulators.

Reverse Taper Review

The reverse taper technique for the suppression of background radiation relies on a large, positive detune [15]

$$\Delta\hat{\nu} = \Delta\nu/2\rho \gg 1, \tag{2}$$

where ρ is the FEL Pierce parameter and $\Delta\nu = (\lambda_r(z) - \lambda)/\lambda$. Note that $\Delta\hat{\nu}$ is the negative of the detune parameter $\hat{C}$ used by Schneidmiller and Yurkov [1]. With Eq. 2 satisfied, the growth of the scaled field intensity $|a|^2 = P/\rho P_{\mathrm{beam}}$ is suppressed in favor of the bunching b,

$$|b|^2 \approx \Delta\hat{\nu}^2|a|^2. \tag{3}$$

This relation is precisely what is desired of a planar undulator upstream from a helical afterburner – strong bunching allows the helical undulator to produce a significant amount of radiation, but background radiation is suppressed.

To satisfy Eq. 3 along the length of the planar undulator, a reverse linear taper (da_u/dz = constant > 0) is introduced so that

$$\Delta\hat{\nu}(\hat{z}) = \beta\hat{z} = \frac{\lambda_u}{4\pi\rho^2}\frac{a_u(0)}{1+a_u(0)^2}\frac{da_u}{dz}\hat{z}, \tag{4}$$

where $\hat{z} = 4\pi\rho z/\lambda_u$ and $a_u(0)$ is the undulator parameter at the start of the planar undulator. The bunching spectrum evolution for a sample reverse taper configuration is shown in Fig. 2. The white line guides the eye by showing how $\Delta\hat{\nu}_0 = (\lambda_r(0) - \lambda_r(z))/2\rho\lambda_r(z)$ changes along a reverse taper, and the bunching intensity is shown to peak close to the initial resonant frequency rather than following the reverse taper. An afterburner would be placed at $z = 45$ and $\Delta\hat{\nu}_0 = -2$ for maximum gain.

1D Simulation Comparison

We have performed 1D simulations to compare the effectiveness of the reverse taper configuration relative to other afterburner schemes. Relevant simulation parameters are included in Table 1. Note that the Pierce parameter for a planar undulator is different than that of a helical undulator due to the presence of the [JJ] factor for planar undulators. The value of ρ_{planar} corresponds to gain length of 1.8 m, within the 1.5-2 m gain length range typically observed at LCLS for 1 keV operation.

Four different afterburner schemes were tested to optimize the degree of circular polarization. Each setup is modeled after the configuration in Fig. 1. A 1D SASE algorithm is used to calculate the beam and radiation conditions at the end of the the planar undulator. The beam is optimally phase shifted relative to the radiation, and both the beam and radiation are used as inputs for the Delta undulator. At the end of the Delta undulator, the power and degree of circular polarization are calculated. Planar undulator segments are assumed to produce plane polarized radiation, while helical undulators are assumed to produce circularly polarized radiation.

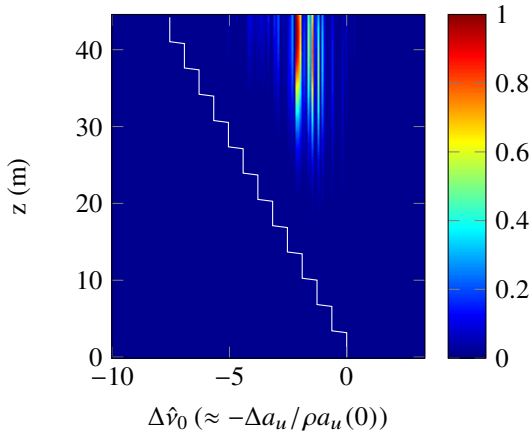

Figure 2: The bunching spectrum in arbitrary units along a reverse tapered 13 undulator line with $\rho = 7.5\times10^{-4}$, $\Delta E/E = 2.5\times10^{-4}$, and $\beta = 0.55$. The x-axis is the detune from $\lambda_r(0)$, and the white line indicates the detune of $\lambda_r(z)$ from $\lambda_r(0)$. Bunching increases with z, but peak bunching does not follow the taper. An afterburner would be placed at $z = 45$ and $\Delta\hat{\nu}_0 = -2$.

Table 1: 1D Simulation Parameters

Parameter	**Value**
x-ray energy	1 keV
beam energy	4.72 GeV
undulator period	3 cm
peak current	1.3 kA
planar undulator segment	3.42 m
Delta undulator	3.2 m
σ_E/E	2.5×10^{-4}
ρ_{planar}	7.5×10^{-4}
ρ_{helical}	9.1×10^{-4}

Figure 3 shows the comparative effectiveness of each scheme. In the first column, a reverse tapered planar undulator is followed by a helical afterburner. The reverse taper does an excellent job suppressing the field growth, and the afterburner is optimally positioned in a_u (c.f. Fig. 2) for rapid field growth. The second column shows a different scheme, wherein an $\hat{x}$ planar undulator is followed by a carefully placed $\hat{y}$ undulator. A $\pi/2$ phase shift between the two produces circularly polarized radiation, but s_3/s_0 is limited by beam slippage [13]. The third column shows the simplest scheme, where a planar undulator is followed by a helical undulator. Proper longitudinal placement of the helical undulator maximizes the power contrast. The final column shows an entirely different scheme, where the beam energy is decreased so that the 2$^{\mathrm{nd}}$ harmonic is 1 keV. The bunched beam is sent into a helical afterburner tuned to 1 keV. A monochromator would be needed to remove the contaminant 500 eV radiation from the circularly polarized 1 keV radiation.

ISBN 978-3-95450-133-5

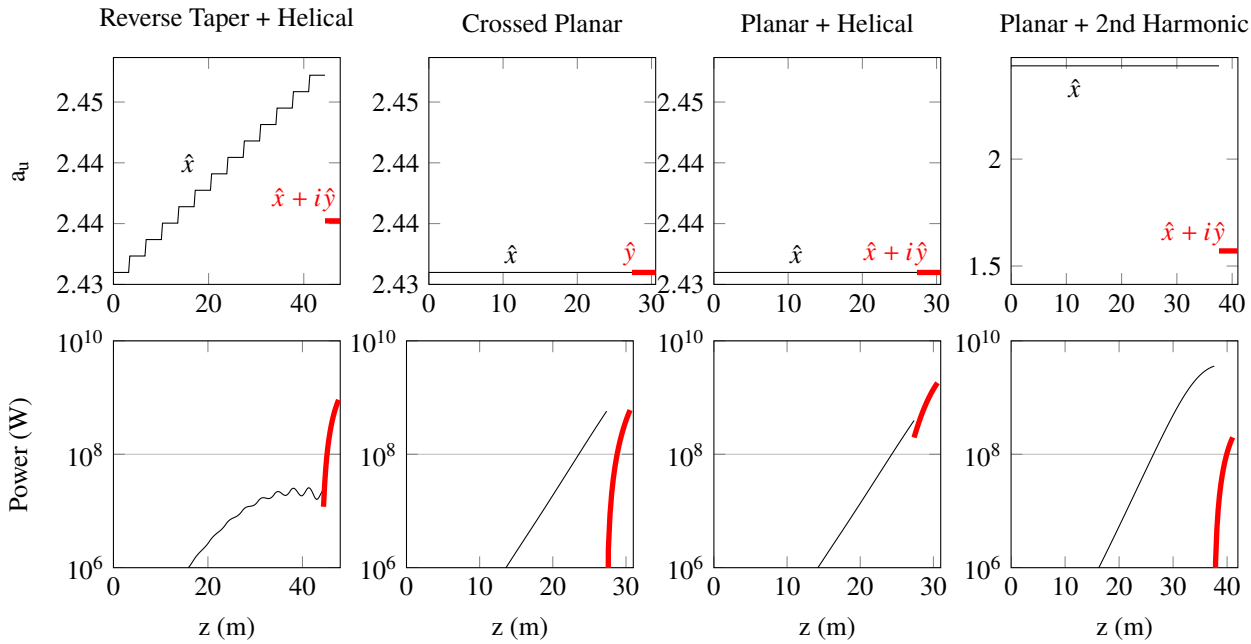

Figure 3: Several schemes for generating circularly polarized radiation are compared. The top row shows the undulator parameter a_u as a function of distance along the undulator for each scheme, with labels indicating whether the radiation produced in the undulator is planar or helical. The bottom row shows the z dependent power produced in the long planar undulator (black) and the afterburner (red).

Table 2 shows summary statistics for each of the afterburner schemes. The reverse taper arrangement provides an ideal balance of power and contrast. These apparent advantages were the basis for a machine study at LCLS, presetned in the next section.

Table 2: Simulation Results

Configuration	Power (GW)	s_3/s_0
Reverse Taper + Helical	0.89	0.975
Cross Planar	0.85	0.829
Planar + Helical	1.80	0.797
Planar + 2nd Harmonic	0.19	1.0

REVERSE TAPER AT LCLS

The Delta undulator is not available to verify these 1D predictions, but the reverse taper concept has been tested at LCLS with a planar afterburner. While no circularly polarized radiation is produced, the x-ray yield contrast before and after the afterburner can verify whether the concept works.

The experimental parameters for the machine study are shown in Table 3. Several different taper slopes and lengths were attempted, and the best configuration is shown in Fig. 4. The contrast was maximized by scanning the afterburner along available a_u values.

The reverse taper was proven to be effective at suppressing unwanted radiation while enabling bunching. As seen in Fig. 5, a contrast of 15 was observed between the end of the taper and the afterburner. Ignoring interference effects, a factor of 15 corresponds to $s_3/s_0 = 0.91$. If the afterburner were helical rather than planar, simulations predict a roughly factor of 2 increase in contrast, equivalent to $s_3/s_0 = 0.95$. This is not far from the prediction in Table 2.

Table 3: Experimental Parameters

Parameter	Value
x-ray energy	1.017 keV
beam energy	4.72 GeV
undulator period	3 cm
peak current	1.3 kA
bunch charge	150 pC
σ_E/E	$\sim 2.5 \times 10^{-4}$
planar undulator segment	3.42 m
standard taper L_G	1.49 m

We could not perform an exhaustive search for the best taper length and slope, and 1D simulations suggest we missed the mark on the ideal taper length. In Fig. 6, the z-dependent bunching spectrum along the undulator configuration of Fig. 4 is simulated using the parameters of Table 3. The ideal location for an afterburner is at peak bunching, which occurs after only 8 undulator segments in the simulation.

Subsequent machine time spent on improving upon these results were met by significantly different beam conditions. The standard taper gain length of the results presented here was 1.49 m, while gain lengths in subsequent experiments were $\geq$ 2 m. Similar contrast could not be achieved with

ISBN 978-3-95450-133-5

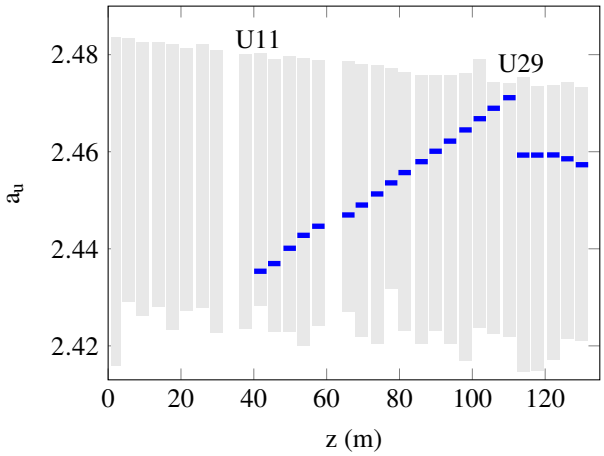

Figure 4: Undulator parameter values for the reverse taper experiment (blue), with available a_u in the background (gray). The reverse taper goes from U11-28 with a gap at U16 for hard x-ray self-seeding. The afterburner is U29. The optimum position of position of U29 was determined by scanning from $a_u = 2.44$ to 2.475.

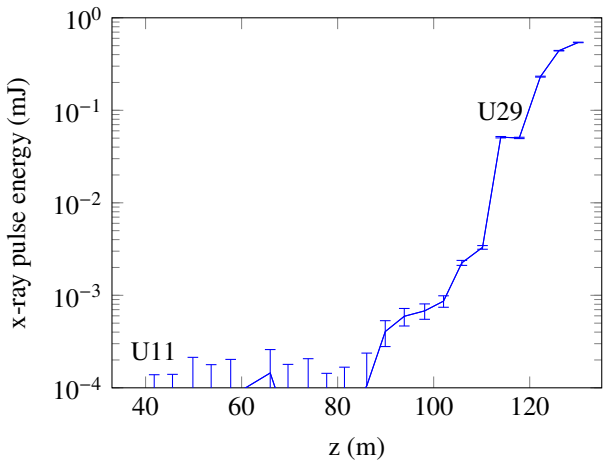

Figure 5: The cumulative pulse energy as a function of distance along the undulator averaged over 120 shots. Between the end of the reverse taper (U28) and the afterburner (U29) the pulse energy increases by a factor of 15.5.

these longer gain lengths in the time allocated to the machine studies. 1D simulations suggest the maximum contrast at acceptable yields is highly dependent upon the energy spread and gain length, so keeping these parameters low will be important during the operation of the Delta undulator.

CONCLUSION

In preparation for the commissioning of the Delta undulator at LCLS, we have performed 1D simulations of different schemes that attempt to maximize the degree of circular polarization and the radiation yield. Machine development time at the LCLS was spent investigating the most promising scheme, a reverse tapered undulator followed by an afterburner undulator. We have achieved a radiation yield contrast

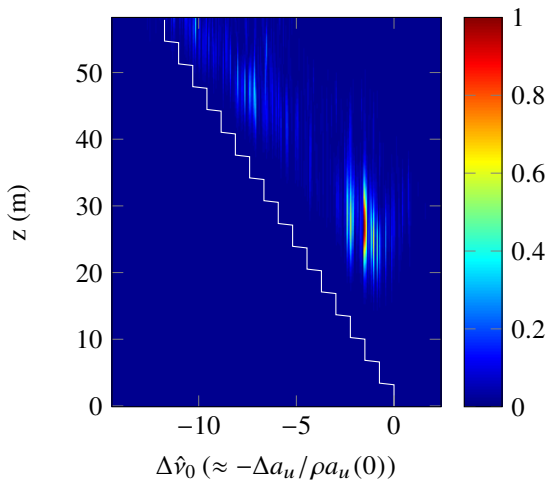

Figure 6: A simulated bunching spectrum to match the experimental parameters. The afterburner U29 would sit at 60 m, but the ideal location for an afterburner may have been earlier. The ideal undulator location is a rather narrow region in $z - \Delta\hat{\nu}_0$ space.

of 15 before and after the afterburner, verifying the utility of this technique. Finding the ideal taper orientation for variable beam conditions may be a challenge, though we expect to learn more during the commissioning of the Delta undulator.

REFERENCES

[1] E. A. Schneidmiller and M. V. Yurkov, "Obtaining High Degree of Circular Polarization at X-ray Free Electron Lasers via a Reverse Undulator Taper," *Phys. Rev. ST Accel. Beams*, vol. 16, p. 110702, 2013.

[2] J. Stöhr *et al.*, "Element-Specific Magnetic Microscopy with Circularly Polarized X-rays," *Science*, vol. 259, pp. 658–658, 1993.

[3] U. Hergenhahn *et al.*, "Photoelectron Circular Dichroism in Core Level Ionization of Randomly Oriented Pure Enantiomers of the Chiral Molecule Camphor," *J. Chem. Phys.*, vol. 120, no. 10, pp. 4553–4556, 2004.

[4] C. T. Chen *et al.*, "Soft-x-ray Magnetic Circular Dichroism at the $l_{2,3}$ Edges of Nickel," *Phys. Rev. B*, vol. 42, pp. 7262–7265, 1990.

[5] S. Sasaki *et al.*, "First Observation of Undulator Radiation from APPLE-1," *Nucl. Instr. Meth. Phys. Res. A*, vol. 347, pp. 87-91, 1994.

[6] T. Mazza *et al.*, "Determining the Polarization State of an Extreme Ultraviolet Free-Electron Laser Beam Using Atomic Circular Dichroism," *Nat. Commun.*, vol. 5, 2014

[7] T. Wang *et al.*, "Femtosecond Single-Shot Imaging of Nanoscale Ferromagnetic Order in Co/Pd Multilayers Using Resonant X-ray Holography," *Phys. Rev. Lett.*, vol. 108, p. 267403, 2012.

[8] A. B. Temnykh, "Delta Undulator for Cornell Energy Recovery Linac," *Phys. Rev. ST Accel. Beams*, vol. 11, p. 120702, 2008.

ISBN 978-3-95450-133-5

[9] H.-D. Nuhn *et al.*, "R&D Towards a Delta-Type Undulator for the LCLS," in *FEL2013 Proceedings*, p. 348, 2013.

[10] R. Carr, "Adjustable Phase Insertion Devices as X-ray Sources," *Nucl. Instr. Meth. Phys. Res. A*, vol. 306, pp. 391–396, 1991

[11] *Principles of Optics*, (New York: Permagon Press, 1964).

[12] K. J. Kim, "A Synchrotron Radiation Source With Arbitrarily Adjustable Elliptical Polarization," *Nucl. Instr. Meth. Phys. Res. A*, vol. 219, no. 2, pp. 425 – 429, 1984.

[13] H. Geng, Y. Ding, and Z. Huang, "Crossed Undulator Polarization Control for X-ray FELs in the Saturation Regime," *Nucl. Instr. Meth. Phys. Res. A*, vol. 622, no. 1, pp. 276 – 280, 2010.

[14] Z. Huang and S. Reiche, "Generation of GW-Level, Sub-angstrom Radiation in the LCLS Using a Second-harmonic Radiator," in *FEL2004 Proceedings*, pp. 201–204, 2004.

[15] Z. Huang and K.-J. Kim, "Review of X-ray Free-Electron Laser Theory," *Phys. Rev. ST Accel. Beams*, vol. 10, p. 034801, 2007.

ISBN 978-3-95450-133-5